Solution-State Structure of the Dewar Pyrimidinone Photoproduct of Thymidylyl-(3′→5′)-thymidine†

John-Stephen Taylor,*,‡ Daniel S. Garrett, and Michael P. Cohrs
Department of Chemistry, Washington University, St. Louis, Missouri 63130
Received January 21, 1988; Revised Manuscript Received May 25, 1988

ABSTRACT: The preparation, spectroscopic investigation, structure determination, conformational analysis, and modeling of the Dewar pyrimidinone photoproduct of thymidylyl-(3′→5′)-thymidine, previously referred to as TpT3 [Johns, H. E., Pearson, M. L., LeBlanc, J. C., & Heilleiner, C. W. (1964) *J. Mol. Biol. 9*, 503-524], is described. TpT3 was prepared in quantitative yield by photolysis of an aqueous solution of the (6-4) photoproduct of TpT with Pyrex-filtered medium-pressure mercury arc light. TpT3 was analyzed by FAB MS, IR, UV, and ^{1}H, ^{13}C, and ^{31}P NMR spectroscopy. The spectroscopic data led to the conclusion that TpT3 results from the photoisomerization of the pyrimidinone ring of the (6-4) product of TpT to its Dewar valence isomer. Torsion angle and interproton distance information derived from coupling constants and NOE data was used to constrain ring conformation searches by utilizing the SYBYL molecular modeling program subroutine SEARCH. Sets of angles derived from the ring search procedure were then used to construct structures whose geometries were optimized by the energy-minimization subroutine MAXIMIN. A two-state model for the solution-state structure of the Dewar photoproduct was chosen which was energetically sound, fit the experimental coupling constants with an RMS deviation of 1.15 Hz, and was consistent with the NOE data. The model for the Dewar photoproduct was compared to a model for the (6-4) photoproduct and the TpT subunits of the Dickerson dodecamer structure by a least-squares fitting procedure. It was concluded that the Dewar photoproduct more closely resembles a B-form TpT unit than does the (6-4) photoproduct.

The cis-syn cyclobutane and (6-4) dipyrimidine dimers are the major photoproducts produced by exposure of duplex DNA to 254-nm light (Wang, 1976). As a result, much work and debate have focused on correlating cis-syn cyclobutane and (6-4) dipyrimidine dimers with ultraviolet light induced mutations (Franklin & Haseltine, 1986; Hutchinson, 1987). Evidence has accumulated over the past 25 years, however, to suggest that (6-4) products are not the ultimate photoproducts produced on exposure of DNA to sunlight. In 1970, type III photoreactivation of some of the lethal effects of 254-nm irradiation in *Streptomyces griseus* and *Streptomyces coelicolor* (Jagger et al., 1970) and *Staphylococcus epidermidis* (Ikegnaga et al., 1970) was discovered. The effectiveness of this type of photoreactivation was shown to be maximal at 313 nm and to proceed through an unknown, though nonenzymatic, pathway that was correlated with the disappearance of (6-4) products (Patrick, 1970; Ikenaga et al., 1970, 1971). Later studies with photolesion-specific RIAs[1] confirmed the photochemical action of 313-nm light on (6-4) products (Mitchell et al., 1985) and led to a polyclonal RIA for their further photolysis products (Mitchell & Rosenstein, 1987). Interestingly, in 1964 it was shown that the (6-4) product of TpT, known then only as TpT4, could be converted quantitatively at 313 nm to a new photoproduct, TpT3, and back again to TpT4 at 240 nm (Johns et al., 1964) (see Figure 1). In 1987 the structure of TpT3 was determined to be the Dewar pyrimidinone valence isomer of the (6-4) product (Taylor & Cohrs, 1987). It was also determined that direct irradiation of TpT with stimulated sunlight led only to the cis-syn, trans-syn, and Dewar photoproducts and no detectable (6-4) product. All the available data suggest that the first step in type III photoreactivation involves the conversion of (6-4) photoproducts to their Dewar pyrimidinone valence isomers. Why the Dewar valence isomers would be less lethal than the (6-4) products is unknown. The available data also suggest that the Dewar photoproducts are produced in significant amounts upon direct exposure of DNA to wavelengths between 280 and 360 nm and thus may be involved in the mechanism of sunlight-induced mutagenesis and skin cancer.

Herein we report the detailed spectroscopic, conformational, and molecular modeling analysis of TpT3. A model of the Dewar photoproduct that best fits the NMR data is then compared to a model of the (6-4) product and B-form TpT in an effort to understand the role that structure might play in type III photoreactivation.

Experimental Procedures

Materials and Methods. Doubly distilled water was used for photolysis and HPLC. Activated carbon used for desalting was Darco G-60. Preparative photolysis was conducted in a Pyrex immersion well reactor with a 450-W medium-pressure mercury arc lamp. Reverse-phase C_{18} chromatography was performed on a Waters μBondapak C_{18} column (3.9 mm × 30 cm, 5-μm μPorasil support, 10% C_{18} plus a trimethylsilyl cap). Gradient HPLC was performed on a system composed of two Waters Series 6000 pumps, a Rheodyne 7125 loop-type

† This investigation was supported in part by USPHS Grant RO1-CA40463, awarded by the National Cancer Institute, USDHHS, and the donors of the Petroleum Research Fund, administered by the American Chemical Society.
‡ Alfred P. Sloan Foundation Fellow.

[1] Abbreviations: RIA, radioimmunoassay; TpT, thymidylyl-(3′→5′)-thymidine; HPLC, high-pressure liquid chromatography; NOE, nuclear Overhauser enhancement; TOE, truncated driven NOE; UV, ultraviolet; IR, infrared; FAB MS, fast atom bombardment mass spectrometry; TSP, 3-(trimethylsilyl)propionic acid sodium salt; DQF COSY, double quantum filtered homonuclear scalar-correlated spectroscopy; RMS, root mean square.

0006-2960/88/0427-7206$01.50/0

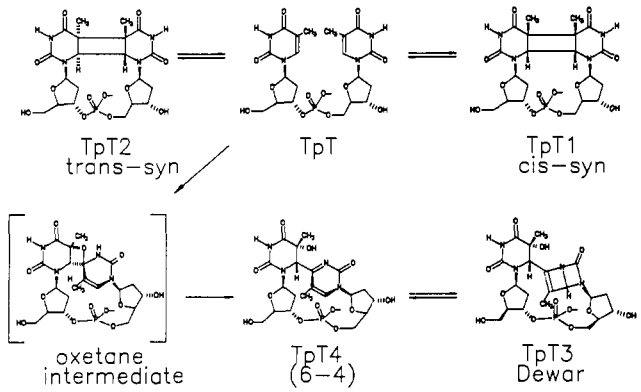

FIGURE 1: Reaction scheme for photolysis of TpT. TpT*n* refer to labels previously assigned to these products (Johns et al., 1964). Structures for the photoproducts come from various sources: cis-syn (Hruska et al., 1975), trans-syn (Liu & Yang, 1978), (6–4) (Rycyna & Alderfer, 1985), and Dewar (Taylor & Cohrs, 1987).

sample injector, and an ISCO V-4 variable-wavelength detector with a 5-mm path length heat exchanger HPLC flow cell. Gradient formation was controlled by an Apple IIe based system, incorporating an Adalab data acquisition card, Chromadapt interface module, and Chromatochart software. KBr matrix IR spectral data were acquired on a Perkin-Elmer 283B calibrated with polystyrene. Mass spectral data were acquired on a VG ZAB-SE double-focusing mass spectrometer equipped with an 8-KeV xenon fast atom bombardment source. ^{1}H (300-MHz) and ^{13}C (75.4-MHz) NMR experiments were performed on a Varian XL-300 instrument with a 5-mm broad-band switchable probe. High-resolution 500-MHz NMR experiments were conducted on a Varian VXR-500 instrument with a 5-mm high-resolution ^{1}H/^{19}F probe. "100%" D_2O was obtained from Merck Sharpe and Dohme Isotopes and was 99.96% D. Molecular mechanics and modeling calculations were performed on a VAX 11/780 with the SYBYL program, release 3.5, from Tripos Associates, St. Louis, MO.

Preparation of TpT3. Approximately 20 mg of the ammonium salt of the (6–4) photoproduct of TpT (Rycyna & Alderfer, 1985) in 100 mL of water was photolyzed for 45 min in an Ace Glass Pyrex immersion well photochemical reaction vessel under tap water cooling. The water was removed under high vacuum in a rotary evaporator to yield TpT3 as a glassy material in quantitative yield.

Analytical C_{18} HPLC. Effluent from a 30-min, 1.0 mL/min, 0–40% linear methanol ramp in 75 mM aqueous KH_2PO_4/K_2HPO_4, pH 7.0, was monitored at 230 nm. Resolution of mixtures containing TpT3 and the cis-syn product of TpT often depended on the quality and age of the column used. Authentic samples of the cis-syn and trans-syn compounds were obtained by acetophenone-sensitized photolysis of TpT (Liu & Yang, 1978) followed by preparative C_{18} HPLC purification and characterization by NMR.

Mass Spectrometry. The purified ammonium salt of TpT3 was suspended in both thioglycerol and triethanolamine for negative ion FAB MS analysis.

NMR Spectroscopy. The ammonium salt of TpT3 was evaporated three times from D_2O on a Speedvac followed by dissolution in "100%" D_2O. TOE difference ^{1}H NMR spectra were obtained according to the general protocol given in the Varian XL-300 Series NMR Spectrometer System Advanced Operation Manual (1984) with some modification. Peak irradiation was conducted at the lowest power level required for complete saturation of the signal in a 4-s time period and was followed after 10 ms by a 40° observe pulse and 2 s of data acquisition. On-resonance transients were interleaved with 2500-Hz off-resonance transients in blocks of 16. The 8K-point FID of the off-resonance experiment was subtracted from that of the on-resonance experiment, zero filled to 16K points, and Fourier transformed with 0.8-Hz line broadening. A heteronuclear scalar-correlated ^{1}H-^{13}C NMR spectrum was obtained by acquiring 128 2K-point FIDs, zero filling to 4K points in *F2* and 256 points in *F1*, and sine-bell weighting in both dimensions prior to Fourier transformation. A heteronuclear *J*-resolved ^{1}H-^{13}C NMR spectrum was obtained by acquiring 64 2K FIDs and zero filling to 4K points in *F2* and 128 points in *F1* prior to Fourier transformation.

Spin Simulation. Iterative spin simulation was conducted with the Varian Version 6.1 software which is based on the FORTRAN program LAME, also known as LAOCOON, with magnetic equivalence added.

Conformational Analysis. Values for torsion angles were determined by least-squares fitting of calculated coupling constants to the observed coupling constants by assuming both one- and two-state conformation models utilizing programs written in GWBASIC. For two-state models the following expression for the deviation Δ_i between a calculated, $J_i(\omega n)$, and an observed coupling constant, J_i(obsd), as a function of two independent angles, $\omega 1$ and $\omega 2$, and a weighting factor $f_{\omega 1}$ was used:

$$\Delta_i(\omega 1,\omega 2,f_{\omega 1}) = f_{\omega 1}J_i(\omega 1) + (1 - f_{\omega 1})J_i(\omega 2) - J_i(\text{obsd})$$

where $0° < \omega 1 < \omega 2 \leq 360°$ and $0 < f_{\omega 1} \leq 1$. Coupling constants were calculated for 10° increments of the intersugar torsion angles, 18° increments of the deoxyribose ring phase angles, and 5° increments of the maximum degree of torsion angles. The weighting factor, $f_{\omega 1}$, was varied in increments of 0.1. Those sets of angles and weighting factors that minimized the sum of the squares of the deviations for all the coupling contants involved were then selected. The deoxyribose phase angle *P* and maximum degree of torsion Φ_M were determined by fitting the sugar ring coupling constants, $J_{1'2'}$, $J_{1'2''}$, $J_{2'3'}$, $J_{2''3'}$, and $J_{3'4'}$, to calculated values. The coupling constants for a given *P* and Φ_M were calculated by combined use of modified Karplus equations (Haasnoot et al., 1980) and endocyclic torsion angles obtained from the pseudorotation equation for deoxyribose rings as has been described (de Leeuw & Altona, 1982). The Tpε bond torsion angle was determined by fitting the $J_{TpH3'-P}$, $J_{TpC2'-P}$, and $J_{TpC4'-P}$ coupling constant data to those calculated by equations recently parametrized for this type of bond (Lankhorst et al., 1984). In a similar fashion the $J_{P-pTC4'}$ coupling constant data were used to determine the pTβ bond torsion angle.

Conformation Search and Strategy. Conformation searches and molecular mechanics calculations were conducted with the SYBYL program. In the first step the Dewar pyrimidinone subunit was built with C_6 in the *R* configuration and minimized by utilizing the SYBYL force field parameters and the SIMPLEX minimizer. The Dewar pyrmidinone ring system was then attached to C_6 of the Tp$C_{3'}$-endo nucleoside 3′-phosphate subunit of a previously derived model of the (6–4) product (Taylor et al., 1988). $C_{3'}$-endo and $C_{2'}$-endo deoxyribose sugar rings were attached to N_1 of the Dewar pyrimidinone ring. The ring closure bond was chosen to be the pT$O_{5'}$-P bond. Selected atoms were then removed to speed up the conformation searches. The conformation searches were undertaken in a series of stages with increasingly tighter constraints utilizing the SEARCH subroutine. In this subroutine a set of bonds are systematically rotated at fixed increments within predefined angle ranges and examined for fulfilling predefined distance criteria. The internucleotide backbone, glycosyl, and

Table I: Proton NMR Chemical Shift Data in ppm for the (6–4) and Dewar Products of TpT at 30 °C in D_2O Relative to TSP

ring	$H_{1'}$	$H_{2'}$	$H_{2''}$	$H_{3'}$	$H_{4'}$	$H_{5'}$	$H_{5''}$	CH_3	H_6
Tp									
(6–4)	6.19	1.44	2.15	3.87	3.71	3.97	3.83	1.76	5.09
Dewar	6.30	2.52[a]	2.36[a]	4.56	3.89	*b*	*b*	1.57	4.73
pT									
(6–4)	6.52	3.04	2.60	4.85	4.15	4.01	3.72	2.32	8.00
Dewar	5.64	2.28	2.27	4.49	3.89	*b*	*b*	2.10	5.33

[a] These shifts were assigned on the basis of the interpretation of the coupling constants. [b] Could not be assigned due to a large degree of overlap.

interpyrimidine torsion angles were initially allowed to vary ±30° in 10° increments about the angles derived from the coupling constant analysis. Sugar torsion angles were held constant. Bonds for which no coupling constant or NOE data were available to derive constraints were allowed to vary ±180° in 30° increments. NOE-active proton pairs were constrained to lie between 1.8 and 5.0 Å, and sterically interacting atoms were constrained to lie no closer than 0.8 times the sum of their van der Waals radii. Ring closure atoms were initially constrained to lie within 1.0 Å, and at later stages this constraint was reduced to 0.1 Å.

Final Structures. Selected angle sets which satisfied all the constraints were then used to build structures for final geometry optimization by energy minimization. Energy minimizations were conducted in two stages with the SYBYL subroutine MAXIMIN without inclusion of the electrostatic energy term. In the first stage internal rings were held rigid and only inter-ring torsion angles were allowed to vary. In the second stage unrestricted geometry optimization was allowed to take place until the energy change was less than 0.01 kcal/iteration.

The MAXIMIN force field and parameters have been described (Taylor et al., 1988) and are essentially those of COSMIC (Vinter et al., 1987). Additions and changes to the published parameters are as follows. Atom types are those of Vinter. Stretch [atom types, equlibrium bond length in Å, force constant in kcal/(mol·Å^2)]: 2–6, 1.33, 1300. Bend [atom types, equilibrium angle in degrees, force constant in kcal/(mol·deg^2)]: 1–2–6, 118, 0.04; 6–2–9, 120, 0.024; 6–2–10, 120, 0.026; 6–1–9, 109.5, 0.02; 6–1–15, 109.5, 0.016; 1–6–2, 110, 0.04; 2–6–2, 109.5, 0.04. Out of plane bend [central atom type, attached atom types, force constant in kcal/(mol·deg^2)]: 2, 1–6–2, 0.08; 2, 6–9–11, 0.08. Torsion (atom types, degeneracy, barrier in kcal/mol): 6–2–1–1, 3, 0.126; 6–2–1–15, 3, 0.274; 6–2–2–1, –2, 12.5; 6–1–2–2, –3, 0.126; 6–1–2–1, 3, 0.126.

Final Models. The models that best accounted for the NMR coupling constant data were determined by first calculating the coupling constants for each final structure. The combination of one, two, or three structures that best minimized the RMS deviation between the calculated and observed coupling constants was chosen as the most representative model for the solution-state structure of TpT3.

Results

TpT3 was prepared in quantitative yield by photolysis of the ammonium salt of the (6–4) product of TpT at a concentration of approximately 1 mM. Photolysis of TpT3 with 254-nm light caused its reversion to the (6–4) product as determined by analytical reverse-phase chromatography (Figure 2B). For comparison purposes the cis-syn and trans-syn photoproducts were also chromatographed under the same conditions (Figure 2C,D). The retention times of the photoproducts were as follows: Dewar, 4.8 min; cis-syn, 5.0 min; (6–4), 9 min; trans-syn, 10.1 min.

Negative FAB MS analysis of TpT3 was conducted in both thioglycerol and triethanolamine matrices. The molecular ion,

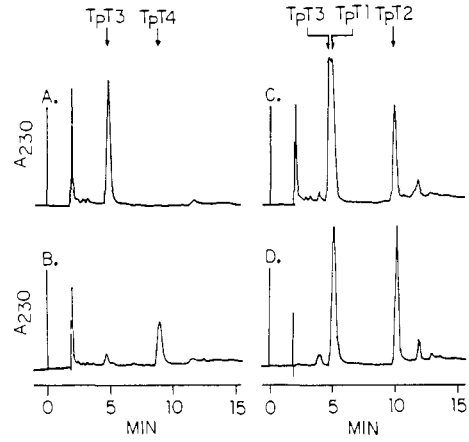

FIGURE 2: Reverse-phase HPLC chromatograms of (A) TpT3, (B) mixture that results from photolysis of TpT3 at 254 nm, (C) coinjection of TpT1, TpT2, and TpT3, and (D) coinjection of TpT1 and TpT2. See Experimental Procedures for details.

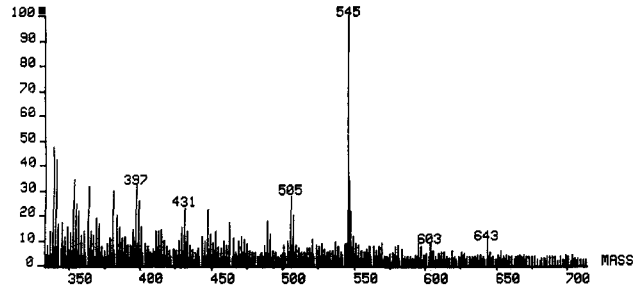

FIGURE 3: Negative ion FAB MS of TpT3 in thioglycerol matrix.

M^-, in the negative ion mode (Figure 3) was determined to have a mass of 545.1294 ± 0.003 by peak matching to glycerol cluster of mass 551.2757 (M_r of TpT3 = 1.011275 × GLC_6 – H^+). The experimentally determined mass deviates by 1.4 × 10^{-3} mass units, or 2.6 ppm, from the mass of 545.1280 calculated for $C_{20}H_{24}N_4O_{12}P$.

The UV spectrum of TpT3 was essentially identical with that originally reported (Johns et al., 1964). The principal change in the UV spectrum on going from the (6–4) product to TpT3 is the loss of the absorption maximum at 325 nm. The most signifiant feature in the IR spectrum of TpT3 is an absorption band at 1780 cm^{-1} which is absent in the spectrum of the (6–4) photoproduct of TpT (Figure 4). TpT3 has a ^{31}P peak at –3.5 ppm at 30 °C in accord with a previous report (Rycyna & Alderfer, 1985).

The 300-MHz ^1H NMR spectrum of TpT3 at 30 °C is shown in Figure 5. The proton chemical shifts are tabulated in Table I and were determined by analysis of absolute-value DQF COSY spectra and decoupling experiments (not shown). The ^1H–^1H coupling constants (Table II) for the $H_{1'}$–$H_{2'}$–$H_{2''}$–$H_{3'}$–$H_{4'}$ network were determined by analysis of decoupling experiments and by iterative spin simulation of the ^1H NMR spectra at 30 and 45 °C, at both 300- and 500-MHz proton frequencies. Coupling constants for the pT sugar ring at 30 °C were confirmed by analysis of the proton spectrum

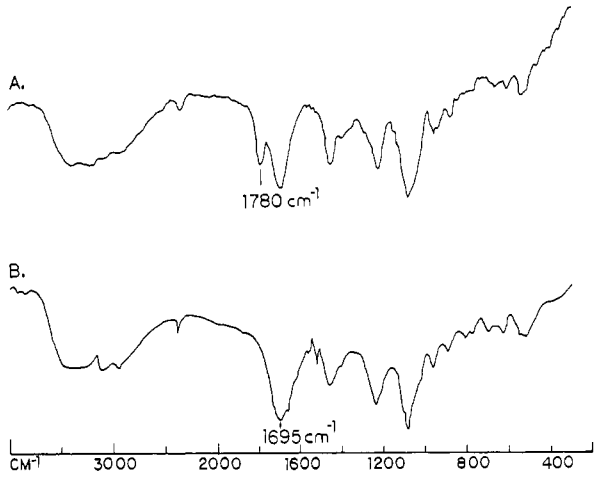

FIGURE 4: IR spectra of (A) TpT3 and (B) the (6–4) product of TpT in a KBr matrix.

at 45 °C, a temperature at which the pT $H_{2'}$ and $H_{2''}$ chemical shifts were no longer degenerate. The $H_{5'}$ and $H_{5''}$ proton signals and associated coupling constants could not be assigned accurately due to the high degree of signal overlap in that region of the spectrum even at a proton frequency of 500 MHz. TOE difference spectra for the four proton NMR singlets are shown in Figure 6.

The ^{13}C NMR chemical shifts (Table III) were assigned by analysis of the heteronuclear scalar-correlated ^1H-^{13}C NMR spectrum (Figure 7) and nondecoupled ^{13}C NMR spectra. The quaternary carbons were tentatively assigned on the basis of the long-range ^{13}C-^1H coupling patterns and by comparison to the assignments made for the (6–4) product. One-bond ^1H–^{13}C coupling constants were obtained directly from both nondecoupled ^{13}C NMR spectra and a heterocorrelated J-resolved ^1H-^{13}C NMR spectrum (expanded section in Figure 8). ^{13}C–^{31}P coupling constants were obtained directly from proton-decoupled ^{13}C NMR spectra.

One- and two-state conformational analysis of Tpε and pTβ torsion bonds were conducted by least-squares fitting of calculated to experimental coupling constants. A minimum deviation of 0.8-Hz RMS between calculated and observed values for $J_{H3'-P}$, $J_{C2'-P}$, and $J_{C4'-P}$ was obtained for a one-state model of 230° for Tpε. A minimum deviation of 0.2-Hz RMS between calculated and observed values for $J_{P-C4'}$ was obtained for a one-state model of either 140° or 220° for pTβ. Both Tpζ and pTα were determined to be in the ±g range on the basis of the ^{31}P NMR shift. The glycosyl bonds and the interpyrimidine bond were all in the −g range as determined by analysis of the NOE data.

Table II: Coupling Constants for the (6–4) and Dewar Products of TpT

ring	$H_{1'-2'}$	$H_{1'-2''}$	$H_{2'-2''}$	$H_{2'-3'}$	$H_{2''-3'}$	$H_{3'-4'}$	
Tp							$H_{3'}$–P
(6–4)[a]	1.5	8.9	−14.1	7.6	11.1	9.2	9.2
Dewar[b]	1.9	9.6	−14.5	8.5	9.6	8.6	9.3
fit[c]	2.6	8.7		7.8	9.2	8.4	9.2
model[d]	2.5	8.6		7.5	9.7	8.5	9.0
deviation[e]	0.6	1.0		1.0	0.1	0.1	0.3
pT							$H_{4'}$–P
(6–4)[a]	3.1	7.6	−15.0	6.9	7.0	4.6	3.3
Dewar[f]	7.0	7.3	−14.1	5.4	7.8	5.8	*g*
fit[c]	5.5	7.3		6.2	6.5	5.7	
model[d]	5.2	7.2		6.4	6.9	6.1	
deviation[e]	1.8	0.1		1.0	0.9	0.3	

[a] Rycyna & Alderfer, 1985. [b] Iterative spin simulation results; RMS fit of 0.36 Hz. [c] Calculated coupling constants for the one- or two-state conformation model that best fit the experimental data for the Dewar product. [d] Calculated coupling constants for the final model for the Dewar product. [e] RMS deviation between experimental coupling constants of the Dewar product and those calculated for the model. [f] Interative spin simulation results; RMS fit of 0.23 Hz. Assignment of coupling constants involving either $pTH_{2'}$ or $pTH_{2''}$ were based on the best fit of the coupling constant data to a two-state model. The alternate assignment leads to poorly fitted coupling constants. [g] Could not be determined.

One- and two-state conformational analyses of the deoxyribose rings were conducted by least-squares fitting of calculated coupling constants to those obtained experimentally. A minimum deviation of 0.66-Hz RMS between calculated and observed coupling constants of the Tp sugar ring was obtained for a one-state model of the $C_{3'}$-endo class, Φ_M = 35°, P = 27°, hereafter denoted as (35,27). For the pT sugar ring, a minimum RMS deviation of 0.92 Hz between calculated and observed coupling constants was obtained for a two-state model consisting of 65% (40,27) and 35% (40,162), corresponding to the $C_{3'}$-endo and $C_{2'}$-endo conformation classes, respectively. By comparison, the best one-state model for the pT ring resulted in a minimum RMS deviation of 2.26 Hz.

A total of 11 structures were obtained from the constrained conformation search (Figure 9). Five representative structures were selected from the $TpC_{3'}$-endo, $pTC_{3'}$-endo class and three from the $TpC_{3'}$-endo, $pTC_{2'}$-endo class, hereafter referred to as ^3E–^3E and ^3E–^2E respectively. Their geometries were then optimized by energy minimization with MAXIMIN. Energies

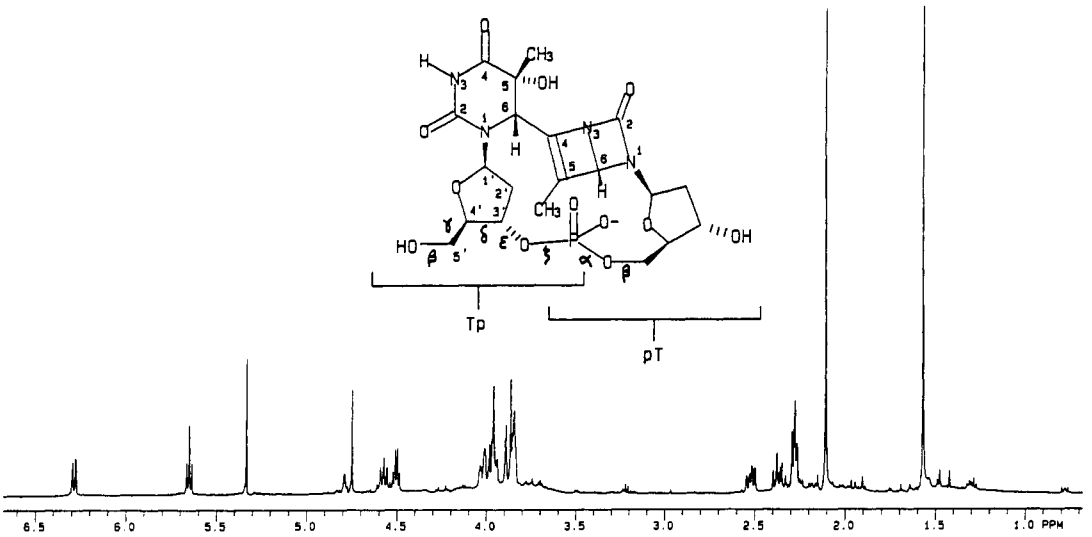

FIGURE 5: 300-MHz proton NMR spectrum of TpT3 at 30 °C in D_2O relative to internal TSP. Labeling shown is used throughout the text.

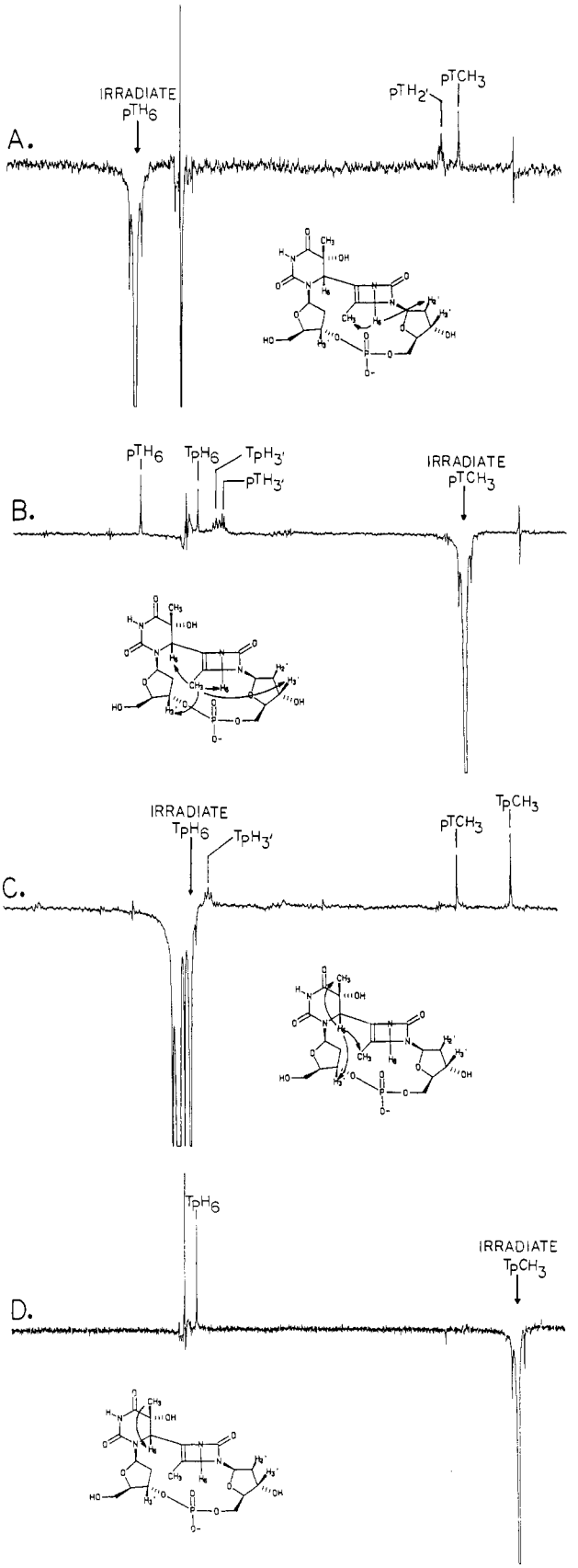

FIGURE 6: TOE difference spectra for the four singlet proton NMR signals of TpT3: (A) pTH6, (B) pTCH$_3$, (C) TpH6, and (D) TpCH$_3$. See Experimental Procedures for details.

for the first class of structures varied from 102 to 110 kcal while those of the second class of structures varied from 100 to 104 kcal. Stereoplots of the two classes of energy-minimized structures are shown in Figure 10. A 65:35 two-state model

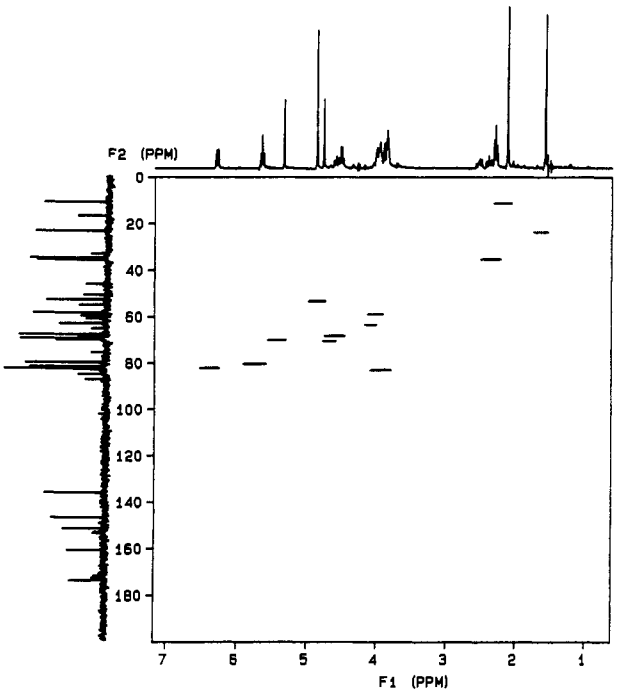

FIGURE 7: 300-MHz heterocorrelated ^{1}H–^{13}C NMR spectrum of TpT3 in D_2O relative to TSP at 30 °C. The sample used for this experiment contained 20% cis-syn dimer whose ^{13}C NMR spectrum is known (Rycyna & Alderfer, 1985) and whose proton signals were subtracted from the 1D proton NMR spectrum shown.

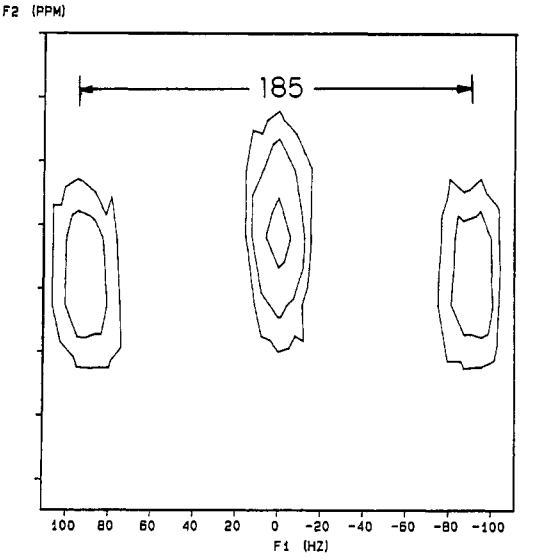

FIGURE 8: Blowup of the heterocorrelated, *J*-resolved ^{1}H–^{13}C NMR spectrum of TpT3. The cross-peak in the center belongs to the quaternary TpC$_5$ carbon.

composed of one of the ^{3}E–^{3}E structures, Tp(37,30)–pT-(38,29), and one of the ^{3}E–^{2}E structures, Tp(37,30)–pT-(37,160), best fit the experimental coupling constant data with a 1.15-Hz RMS deviation. Relevant interproton distances and angles are in Table IV and V.

The average RMS deviation of the TpO$_2$, TpN$_3$, TpO$_4$, TpC$_{2'}$, pTO$_2$, pTN$_3$, P, and pTC$_{2'}$ atomic coordinates was 0.18 Å for the ^{3}E–^{3}E class of structures and 0.16 Å for the ^{3}E–^{2}E class. By use of the same set of atoms, the ^{3}E–^{3}E structure of the Dewar model fit the ^{3}E–$_2$E structure of the two-state (6–4) product model previously proposed (Taylor et al., 1988) with an RMS deviation of 0.88 Å. The ^{3}E–^{2}E structure of the Dewar model fit the ^{3}E–$_3$E structure of the (6–4) model with an RMS deviation of 0.85 Å. A superposition of the individual structures of the Dewar and (6–4) models is shown

Table III: ^{13}C NMR Chemical Shifts in ppm from TSP and One-Bond ^{1}H–^{13}C and Both Three- and Four-Bond ^{31}P–^{13}C Coupling Constants in Hz at 30 °C

	$C_{1'}$	$C_{2'}$	$C_{3'}$	$C_{4'}$	$C_{5'}$	C_2	C_4	C_5	C_6	CH_3
Tp										
(6–4)[a]	84.9	37.5	72.3	84.8	61.4	156.4[b]	176.7[b]	74.9	60.4	27.7
J_{P-C}		3.2	5.4	6.1						
Dewar	84.7	38.0[c]	73.1[d]	85.6[e]	61.6	154.7[f]	177.0[f]	72.4[d]	55.9	26.4
J_{P-C}		2.3	5.4	5.2						
J_{H-C}	169.6	133.8	147.4	146.1	141.7				143.3	129.0
pT										
(6–4)[a]	90.7	37.6	72.5	88.5	67.4	159.9[b]	176.9[b]	119.0	146.8	16.2
J_{P-C}				9.5	5.6					
Dewar	82.9	38.8[c]	70.8	85.5[e]	66.1	163.9[f]	149.9[f]	139.1[f]	72.5[d]	13.9
J_{P-C}				7.5	5.2					
J_{H-C}	168.9	134.5	151.2	146.1	145.5				183.9	129.0

[a] Rycyna & Alderfer, 1985. [b] Assignments may be interchanged within a column. [c] These were distinguished by the ^{31}P coupling in nondecoupled ^{13}C NMR spectra. [d] These were distinguished by analysis of the ^{1}H–^{13}C scalar-correlated J-resolved NMR spectrum. [e] These shifts could not be distinguished due to spectral overlap of the Tp and pT $C_{4'}$ and $H_{4'}$ signals in the heteroscalar-correlated 2D NMR spectra. [f] Tentatively assigned on the basis of analysis of the coupling patterns in nondecoupled ^{13}C NMR spectra.

Table IV: NOE-Active and -Inactive Interproton Distances[a] in Angstroms for the Dewar Photoproduct Model and Its Component Structures

atom 1	atom 2	^3E–^3E	^3E–^2E	model
		NOE Active		
TpH_6	$TpCH_3$	2.9	2.9	2.9
	$TpH_{3'}$	2.2	2.2	2.2
	$pTCH_3$	3.6	3.6	3.6
$pTCH_3$	$TpH_{3'}$	2.7	2.8	2.8
	pTH_6	3.5	3.5	3.5
	$pTH_{3'}$	2.7	5.0	2.9
pTH_6	$pTH_{2'}$	2.7	3.4	2.8
		NOE Inactive (Distance Less Than 4 Å)		
TpH_6	$TpH_{2'}$	3.2	3.2	3.2
$pTCH_3$	$pTH_{2'}$	3.7	2.9	3.3
pTH_6	$pTH_{2''}$	4.2	3.4	3.8

[a] Interproton distances for the model are $1/r^6$ weighted averages; distances to methyl protons are to their centroids.

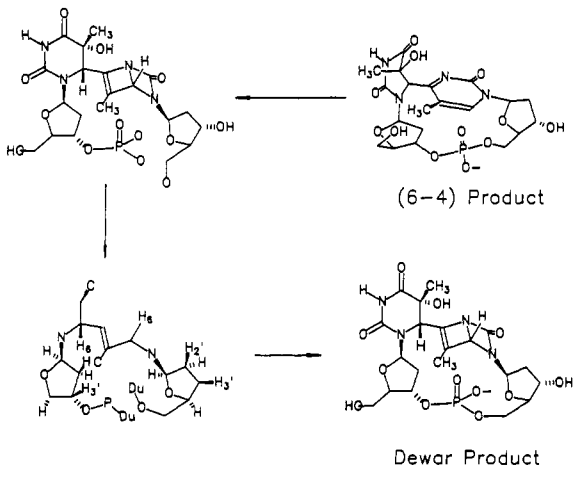

FIGURE 9: Scheme used for obtaining structures for the Dewar photoproduct via the constrained conformation search. Du represents a dummy atom, and C represents a dummy atom at the centroid of the methyl hydrogens.

in Figure 11. The $TpO_{5'}$, $TpC_{5'}$, TpO_2, TpN_3, TpO_4, $TpC_{3'}$, P, $pTC_{3'}$, and $pTO_{3'}$ atomic coordinates of the Dewar model fit those of the T7T8 subunit of the Dickerson dodecamer structure (Dickerson & Drew, 1981) with an RMS deviation of 1.12 Å. In contrast, the (6–4) model only fit with an RMS deviation of 1.65 Å.

DISCUSSION

Chemistry. The photochemical behavior of the (6–4) product as originally described (Johns et al., 1964) is very similar to that of simpler pyrimidinones. It has been shown that 2-pyrimidinones are converted to their Dewar isomers upon irradiation at 313 nm and back again to their pyrimidinone form upon irradiation at 254 nm (Nishio et al., 1978, 1980). Pyrimidinones have a characteristic long-wavelength maximum in the range of 300–330 nm corresponding to an $n \rightarrow \pi^*$ transition. Excitation of this absorption band results in the conversion of pyrimidinones to their Dewar valence isomers which no longer have this band due to the loss of the conjugated π system. As a result, photolysis of pyrimidinones at wavelengths between approximately 290 and 360 nm results in photoequilibrium mixtures composed almost exclusively of the Dewar valence isomers.

Cytosine, a pyrimidinone, is well-known to form thermally unstable hydrates upon exposure to ultraviolet light (Wang, 1976). Unlike photohydrates, TpT3 is stable at 85 °C for 12 h at pH 7 (Johns et al., 1964). The ^{1}H NMR spectrum remains unchanged at 80 °C in D_2O for 0.5 h with no additional proton exchange for deuterium occurring over that which takes place at room temperature. The thermal stability of TpT3 in neutral protic solvent is similar to that of 4,6-dimethyl-1-phenyl Dewar pyrimidinone, which is known to be stable in refluxing methanol (Nishio et al., 1981). The thermal stability of TpT3 suggests that Dewar photoproducts would be stable to the 0.5-h, 90 °C denaturing step routinely used in the photoproduct RIAs (Mitchell & Clarkson, 1981).

Table V: Torsion Angles in deg of Minimized Structures for the (6–4) and Dewar Photoproducts and of TpT Units from the Dickerson Dodecamer Crystal Structure[a]

	(6–4) structures		Dewar structures		Dickerson structure	
angle[b]	^3E–$_2E$[c]	^3E–$_3E$	^3E–^3E	^3E–^2E	T_7–T_8	T_{19}–T_{20}
Tpχ	−138	−149	−129	−129	−127	−68
γ	56	57	76	75	52	60
δ	80	77	82	82	99	109
ϵ	253	261	228	204	174	179
ζ	−76	−85	−77	−57	−86	−88
pTα	−96	−94	−36	−70	−59	−59
β	183	177	157	180	173	179
γ	43	63	4	42	64	55
δ	100	162	84	147	109	122
χ	−75	−44	−56	−37	−126	−120
(6–4)	27	23	56	56		
Me-pyo	−163	−164	−167	−167		

[a] Dickerson & Drew, 1981. [b] Saenger (1984): α, $O_{3'}$–P–$O_{5'}$–$C_{5'}$; β, P–$O_{5'}$–$C_{5'}$–$C_{4'}$; γ, $O_{5'}$–$C_{5'}$–$C_{4'}$–$C_{3'}$; δ, $C_{5'}$–$C_{4'}$–$C_{3'}$–$O_{3'}$; ϵ, $C_{4'}$–$C_{3'}$–$O_{3'}$–P; ζ, $C_{3'}$–$O_{3'}$–P–$O_{5'}$; χ, O_4–C_1–N_1–C_2; (6–4), TpN_1–C_6–pTC_4–N_3; Me-pyo, $TpCH_3$–C_5–C_6–pTC_4. [c] Refers to the conformation class of the Tp and pT sugar rings of a given structure.

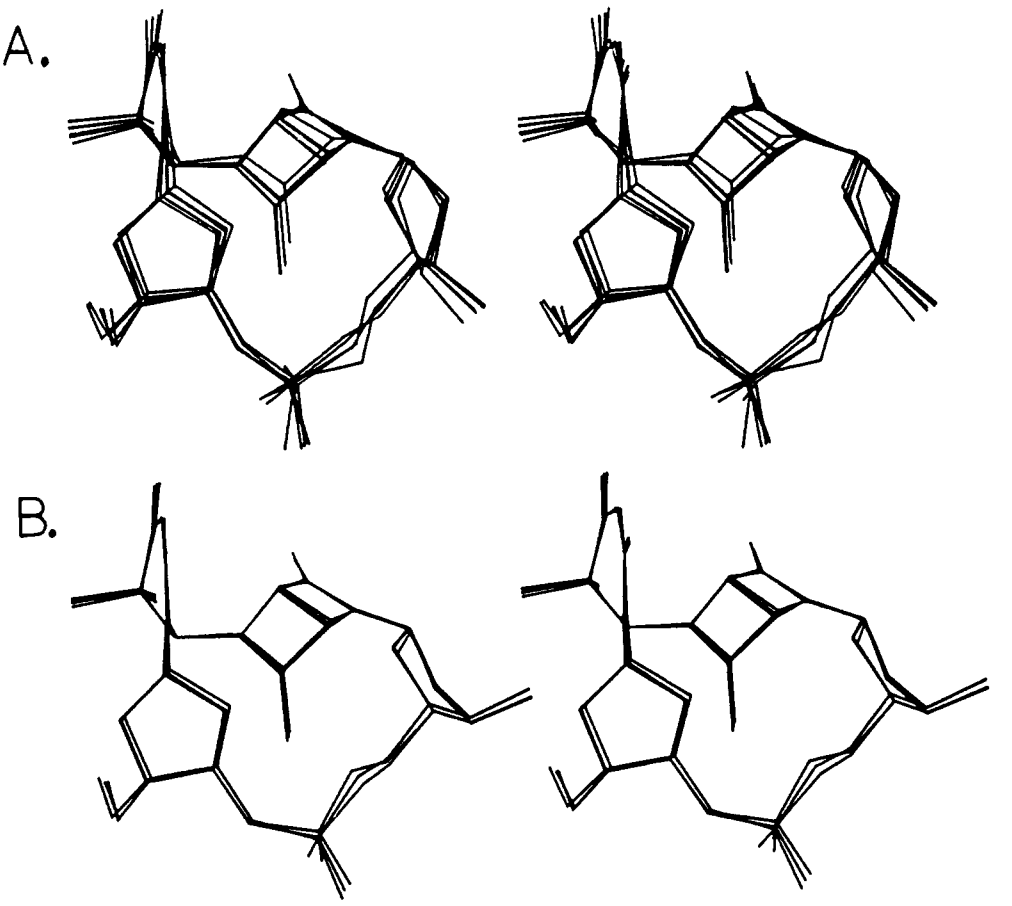

FIGURE 10: Stereoplots of the (A) ^3E–^3E and (B) ^3E–^2E classes of Dewar structures after energy minimization. Atoms fit are listed under Results.

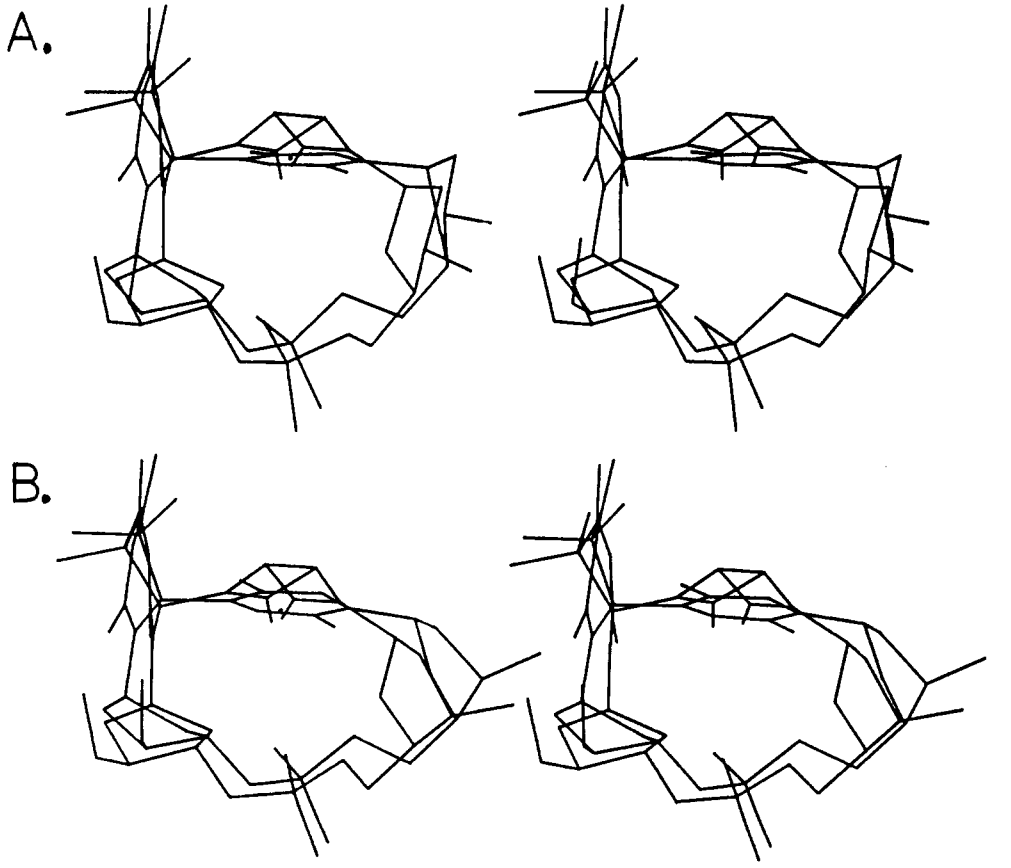

FIGURE 11: Comparison of the component structures of the Dewar and (6–4) models. Stereoplots of (A) the ^3E–^3E Dewar structure and the ^3E–$_2E$ (6–4) structure and (B) the ^3E–^2E Dewar structure and the ^3E–$_3E$ (6–4) structure. Atoms fit are listed under Results.

Therefore, the further photoproducts of the (6–4) products detected by the polyclonal RIA are probably the Dewar products and not degradation products.

In contrast, TpT3 is unstable in 0.1 N KOH at 85 °C for 12 h (Johns et al., 1964). This too is consistent with a Dewar pyrimidinone structure, as 4,6-dimethyl-1-phenyl Dewar pyrimidinone is known to be degraded by a 3-h treatment with 70 mM potassium methoxide in methanol at room temperature (Nishio et al., 1980). The (6–4) products of TpT, TpC, and CpC are also unstable to base, being degraded by 0.1 N KOH at 90 °C for $^1/_2$ h (Franklin et al., 1982). As a result, hot alkali induced cleavage of photolyzed DNA has been used to determine the sites and relative amounts of (6–4) product production (Lipke et al., 1981). The rate of production of alkali-labile sites between 254 and 334 nm was found to parallel that of cis-syn dimer production (Chan et al., 1986). In contrast, the rate of production of (6–4) products determined by RIA was found to be half that of cis-syn dimers at 313 nm (Rosenstein & Mitchell, 1987). Preliminary results also indicated that alkali treatment greatly reduced the antibody binding for the further photoproducts of the (6–4) products. It was suggested that the remainder of the alkali-labile sites induced in DNA by 313-nm light must result from cleavage at sites of the photolysis products of the (6–4) products (Rosenstein & Mitchell, 1987; Mitchell & Rosenstein, 1987). The alkalai cleavage data are consistent with Dewar pyrimdinone structures for the photolysis products of the the (6–4) products since both TpT3 and Dewar pyrimidinones are base degradable.

Spectroscopy. In order to minimize dehydration of a possible photohydrate during FAB MS, the sample was run in both basic and acidic matrices in the negative ion mode (Figure 3). A molecular ion identical in mass with that of the (6–4) product was detected. There was no significant $(M + 18)^-$ peak.

A carbonyl band appears at 1780 cm^{-1} in the IR spectrum of TpT3 which is 30 cm^{-1} higher than that found in the (6–4) product (Figure 4). Dewar pyrimidinones have an absorption band in the 1760–1790-cm^{-1} range corresponding to the four-membered ring cyclic urea carbonyl (Nishio et al., 1980).

The ^{31}P NMR shifts of the four photoproducts of TpT and their temperature dependence have been reported (Rycyna & Alderfer, 1985) and reflect the conformation about the phosphodiester bonds. The close similarity of the chemical shift (−3.46 vs −3.50 ppm at 30 °C relative to TMP) and temperature dependence (approximately 0.0064 vs 0.0043 ppm/°C) of the ^{31}P signals of the (6–4) and TpT3 products strongly suggest similar conformational properties about their phosphodiester bonds. The uniqueness and temperature dependence of the ^{31}P signals of these photoproducts indicate that multiple conformers exist in solution that are in rapid equilibrium relative to the NMR time scale.

The assignments of the proton signals were made possible by analysis of DQF COSY NMR spectra, selective decoupling experiments, and TOE difference proton NMR spectra. The scalar-correlated $H_{1'}$–$H_{2'}$,$H_{2''}$–$H_{3'}$–$H_{4'}$ connectivities for each sugar ring were obtained directly from DQF COSY NMR spectra whereas the assignments of the sugar rings were made by analysis of the TOE difference proton NMR spectra (Figure 6). The singlets at 4.8 and 5.4 ppm correspond to the two H_6 protons. Since irradiation of the H_6 signal at 4.8 ppm led to enhancement of the $H_{3'}$ signal of one of the sugar rings and both methyl signals (Figure 6C), it could be assigned to the Tp sugar ring. In support of this assignment, irradiation of the H_6 signal at 5.4 ppm led to enhancement of the $H_{2'}$ and/or $H_{2''}$ signal of the other sugar ring and only the methyl signal at 2.3 ppm (Figure 6A). Since irradiation of the methyl signal at 2.3 ppm led to enhancement of all the $H_{3'}$ and H_6 signals, it could assigned to the centrally located pT methyl group (Figure 6B). As is the case for the (6–4) product, irradiation of the $TpCH_3$ signal led only to enhancement of the TpH_6 proton and no enhancement of the $pTCH_3$ signal.

The $H_{2'}$ and $H_{2''}$ proton signals, which in the (6–4) product range between 1.44 and 3.04 ppm due to pyrimidinone induced shielding and deshielding effects, range in TpT3 between the more commonly observed values of 2.27 and 2.52 ppm (Table I). In addition, the pTH_6 shift of 5.45 ppm is 2.65 ppm upfield from that found for the (6–4) product. The differences between the proton chemical shifts of the (6–4) product and TpT3 strongly suggest the absence of an aromatic pyrimidinone ring in TpT3. Only five signals appear in the carbonyl and olefin region of the ^{13}C NMR spectrum instead of the six found for the (6–4) photoproduct, indicating that only one of the pyrimidinone carbons had rehybridized (Table III). pTC_6 was identified as the rehybridized carbon by its scalar correlation with the pTH_6 proton (Figure 7). The pTC_6 NMR shift of 72.5 ppm is 74.3 ppm upfield from that of the corresponding carbon in the (6–4) product. The pTC_6–H_6 coupling constant was determined by both nondecoupled ^{13}C NMR spectroscopy and ^1H-^{13}C heterocorrelated *J*-resolved NMR spectroscopy (Figure 8) to be 185 Hz. This unusually high coupling constant corresponds to a C–H bond with 37% s character or a formal hybridization of $sp^{1.7}$ (Shoolery, 1959). The chemical shifts of pTC_6 and pTH_6 together with the large C–H coupling constant is fully consistent with a bridgehead pTC_6 carbon in a small-membered ring heterocycle.

In summary, all the structural changes that take place on going from the (6–4) product to TpT3 can be associated with the pyrimidinone ring and are consistent with photoisomerization of the pyrimidinone ring to its Dewar valence isomer. The stereochemistry of the pTC_6 carbon was assigned as *R* primarily on the basis of the observed NOEs between $pTCH_3$ and both $H_{3'}$ protons and the results of model building, taking into consideration all of the observed interproton NOEs. Models with the *S* configuration were untenable.

Conformational Analysis. The conformation of TpT3 was quite similar to that of the (6–4) product (Taylor et al., 1984) in a number of ways. The Tp sugar ring was determined to best fit a one-state $C_{3'}$-endo-type conformation as was found for the (6–4) product. Two-state models did not significantly improve the RMS deviation between calculated and observed coupling constants. The pT ring presented an unusual set of coupling constants of almost equal magnitude that could be best fit to a two-state model composed of nearly equal proportions of $C_{3'}$-endo- and $C_{2'}$-endo-type conformations. The $C_{3'}$-endo and $C_{2'}$-endo sugar conformations each differ by a phase angle of approximately 36° from the respective $C_{2'}$-exo and $C_{3'}$-exo sugar conformations found for the (6–4) product.

As was the case for the (6–4) product, the conformation about $Tp\epsilon$ could be best described by a one-state model of 230° whereas for $pT\beta$ one-state models of either 140° or 220° could not be distinguished. Conformational analysis of $pT\gamma$ could not be carried out because the required coupling constants could not be determined due to a high degree of signal overlap in this region of the spectrum. Both the phosphodiester bond angles $Tp\zeta$ and $pT\alpha$ were determined to be in $\pm g$ states as had been determined for the (6–4) product of TpT. The glycosyl torsion angles could only be determined qualitatively from the NOE data. The NOE observed between TpH_6 and $TpH_{3'}$ placed the Tp glycosyl angle in the $-g$ range (Figure 6C). The

pT glycosyl angle was also determined to be in the $-g$ range as an NOE was observed between pTH_6 and $pTH_{2'}$ (Figure 6A). The inter-pyrimidine angle, $TpN_1-C_6-pTC_4-C_5$, was determined to be in the $-g$ range as NOEs were observed between $pTCH_3$ and both TpH_6 and $TpH_{3'}$ (Figure 6B).

Molecular Modeling. The SYBYL-minimized Dewar pyrimidinone subunit was found to be quite similar in structure to two crystal structures of Dewar valence isomers (Weinges et al., 1984 and 1986). The 117° flap angle (angle between the two mean planes of the four-membered rings) of TpT3 compares quite favorably with that of 116–117° found in the crystal structures. The exocyclic valence angles of 128° for $TpC_5-pTC_4-N_3$ and 132° for $pTC_6-N_1-C_{1'}$ are also quite similar to crystal structure values of 130°. The most significant differences were found for the lengths of the heteroatom-containing bonds. For example, the bridging pTC_6-N_3 bond length of 1.52 Å is slightly smaller than that of 1.59 Å found for the bridging C–C bond of the all carbon isomers and can be ascribed to the bond-shortening effect of nitrogen relative to carbon. All the other structural parameters compare favorably. The energy difference between the pyrimidinone subunit and its Dewar valence isomer was calculated to be approximately 82 kcal by the SYBYL force field. In comparison, the thermodynamically derived ΔH difference between hexamethylbenzene and its Dewar valence isomer is only 59.5 kcal (Oth, 1968), suggesting that the force field derived value may be an overestimation. The energies of the (6–4) and Dewar structures minus their pyrimidinone subunits are quite similar, indicating that little change in the strain energy of the sugar–phosphate backbone results from the valence isomerization.

In all, eight structures were selected from eleven that were obtained from the constrained conformation search and energy minimized to optimize the van der Waals contacts that were purposefully attenuated during the conformation search. The structures all have minimized energies within 10 kcal of each other, and all are devoid of bad van der Waals contacts, signifying that they are all sterically acceptable. Though the structures differ widely in their minimized energies, they are probably close to their true minima and are acceptable as representative structures for models of the Dewar product.

The Model. The best model for the solution-state structure of the Dewar photoproduct was considered to be that one-, two-, or three-state combination of final structures which minimized the deviation between the experimental and calculated coupling constant data. A rapidly equilibrating two-state model composed of 65% of one of the ^3E–^3E structures and 35% of one of the ^3E–^2E structures fit the proton coupling constant data with an RMS deviation of 1.15 Hz. Inclusion of a third structure did not improve the fit. All the calculated coupling constants deviated by less than 1.0 Hz with the exception of that for $pTH_{1'-2'}$ which deviated by 1.8 Hz (Table II). The large deviation is a consequence of having to mix a small coupling constant of 2.33 Hz for the ^3E–^3E structure and a large coupling constant of 10.5 Hz for the ^3E–^2E structure.

In order to assess the extent to which the two-state model is consistent with the observed NOEs, use was made of the fact that NOE buildup is proportional to the inverse sixth power of the interproton distance (Noggle & Schirmer, 1971). Therefore, $1/r^6$ weighted averages of the interproton distances of the individual structures were calculated (Table IV). In the model all NOE-active distances fall within 3.6 Å whereas only two NOE-inactive distances fall within this range. These two NOE-inactive interproton distances are both greater than 3.1 Å, and it is possible that they would not be observable under the conditions used in the TOE experiments. A complete relaxation matrix analysis of the final model would be necessary to properly evaluate the NOE data.

In summary, the two-state model is energetically sound and consistent with the observed coupling constants, NOEs, and the temperature dependence of the ^{31}P and pT $H_{2'}$ and $H_{2''}$ NMR signals. Though this model is consistent with the experimental data, its uniqueness cannot be ascertained by the method used to obtain it. Such an issue could only be resolved with an unrestricted conformation search followed by energy ranking of the resulting conformers. The number of grossly different structures for the Dewar product is expected to be exceedingly small, however, due to the number of steric and conformational constraints imposed by the five ring systems of the molecule. In this regard, the two structures that make up the Dewar model probably represent two of the major families of structures present in solution and can be used for comparison purposes.

Comparison to the (6–4) Product and B-Form DNA. The two-state model of the Dewar product was compared to the two-state model for the (6–4) product which had been previously derived by a similar constrained search procedure (Taylor et al., 1988). The models for the two photoproducts are quite similar in that they are both composed of a Tp sugar of the $C_{3'}$-endo class and a set of pT sugar rings that equilibrate between $C_{3'}$-endo- and $C_{2'}$-endo-type conformations (Figure 11). They differ perceptibly, however, in the pT portion of the structures. Isomerization of the flat pyrimidinone rings of the (6–4) products to their bent Dewar valence isomers draws the pT sugar rings toward the center of the structures, making the Dewar products more compact. As a result, the Dewar structures fit the T7T8 subunit of the Dickerson dodecamer structure better than do the (6–4) structures, suggesting the Dewar products might cause less distortion of B DNA than do (6–4) products.

One possible consequence of the greater structural similarity of the Dewar product to B DNA than the (6–4) product is that Dewar products might be more easily bypassed by replication systems than the (6–4) products and hence less lethal. Type III photoreactivation could then be explained by the conversion of (6–4) products produced during 254-nm irradiation to the more easily bypassed Dewar products upon irradiation with 313-nm light. Another consequence of the structural differences between the Dewar and (6–4) products might be that Dewar photoproducts are less readily detected by repair systems than are (6–4) products and that this might contribute to greater mutagenicity.

Experimentally, the structural difference between the (6–4) and Dewar photoproducts of TpT is most evident in their chromatographic behavior. The order of elution of compounds from a C_{18} column can generally be correlated with the amount of exposed hydrophobic molecular surface area. The Dewar photoproduct elutes much earlier than the (6–4) product on a reverse-phase column (Figure 2) and has a retention time quite similar to that of the cis-syn product. Earlier studies on TpT photoproducts which employed reverse-phase HPLC as a method of analysis (Franklin et al., 1982; Ulmas et al., 1985) may have missed detecting the Dewar photoproduct as it often coelutes with the cis-syn product (Figure 2C). The (6–4) product, on the other hand, has a retention time similar to that of the trans-syn product. Melting temperature studies on cis-syn and trans-syn containing duplex decanucleotides (Taylor et al., unpublished results) indicate that the trans-syn thymine dimer destabilizes B DNA much more than does the cis-syn thymine dimer. It is possible that a correlation exists

between the retention times of dinucleotide photoproducts and their ability to destabilize DNA duplexes.

Biological Significance. All the available data strongly suggest that the (6–4) products of TpT, TpC, CpC, and CpT sites in DNA are converted to their Dewar valence isomers upon exposure to wavelengths of light between 280 and 360 nm and that this represents the first step in type III photoreactivation. The available data also suggest that Dewar products are produced upon direct exposure of DNA to sunlight via the intermediate (6–4) products and therefore must play a hitherto unrecognized role in sunlight-induced mutagenesis. It is important that conclusions drawn from mutagenesis and enzymological experiments which have involved the use of light between 280 and 360 nm be reevaluated with regard to the photochemistry of the (6–4) products and the properties of their Dewar valence isomers. Of particular concern are conclusions drawn from experiments that have utilized photoreactivating enzymes and long-wavelength light as a method for selectively removing cis-syn dimers from DNA containing (6–4) products. Experiments that have equated hot-alkali cleavage sites with sites of (6–4) products must likewise be reinterpreted, taking into account the likelihood that alkali treatment cannot distinguish between (6–4) and Dewar products.

In summary, a detailed spectroscopic investigation of the photoproduct previously known only as TpT3 has been presented. Interpretation of the spectroscopic data led to the conclusion that TpT3 is the Dewar valence isomer of the (6–4) photoproduct of TpT. Molecular modeling of the structure based on the conformational analysis led to a two-state model for its structure in solution that was energetically sound and consistent with the spectroscopic data. This model was compared to a model of the (6–4) product and B-form TpT. These comparisons led to the conclusion that the Dewar photoproduct more closely resembles B DNA than does the (6–4) product. How these structural differences relate to mechanisms of sunlight-induced mutagenesis and type III photoreactivation remains to be determined.

ACKNOWLEDGMENTS

The assistance of the Washington University High Resolution NMR Service Facility, funded in part through NIH Biomedical Research Support Shared Instrument Grant 1 S110 RR02004 and a gift from the Monsanto Co., is gratefully acknowledged. We thank Dr. Andrew Tyler for acquiring the fast atom bombardment mass spectrometry data at the Washington University Spectrometry Resource, supported by a grant from the NIH (RR00954).

REFERENCES

Chan, G. L., Peak, M. J., Peak, J. G., & Haseltine, W. A. (1986) *Int. J. Radiat. Biol. Relat. Stud. Phys., Chem. Med. 50*, 641–648.

De Leeuw, F. A. A. M., & Altona, C. (1982) *J. Chem. Soc., Perkin Trans. 2*, 375–384.

Dickerson, R. E., & Drew, H. R. (1981) *J. Mol. Biol. 149*, 761–786.

Franklin, W. A., & Haseltine, W. A. (1986) *Mutat. Res. 165*, 1–7.

Franklin, W. A., Lo, K. M., & Haseltine, W. A. (1982) *J. Biol. Chem. 257*, 13535–13543.

Franklin, W., Doetsch, P. W., & Haseltine, W. A. (1985) *Nucleic Acids Res. 13*, 5317–5325.

Gorenstein, D. G. (1984) *Phosphorus-31 NMR, Principles and Applications* (Gorenstein, D. G., Ed.) pp 7–36, Academic, New York.

Haasnoot, C. A. G., De Leeuw, F. A. A. M., & Altona, C. (1980) *Tetrahedron 36*, 2783–2792.

Hruska, F. E., Wood, D. J., Ogilvie, K. K., & Charlton, J. L. (1975) *Can. J. Chem. 53*, 1193–1203.

Hutchinson, F. (1987) *Photochem. Photobiol. 45*, 897–903.

Ikenaga, M., Patrick, M. H., & Jagger, J. (1970) *Photochem. Photobiol. 11*, 487–494.

Ikenaga, M., Patrick, M. H., & Jagger, J. (1971) *Photochem. Photobiol. 14*, 175–187.

Jagger, J., Takebe, H., & Snow, J. M. (1970) *Photochem. Photobiol. 12*, 185–196.

Johns, H. E., Pearson, M. L., LeBlanc, J. C., & Helleiner, C. W. (1964) *J. Mol. Biol. 9*, 503–524.

Lankhorst, P. P., Haasnoot, C. A. G., Erkelens, C., & Altona, C. (1984) *J. Biomol. Struct. Dyn. 1*, 1387–1405.

Lipke, J. A., Gordon, L. K., Brash, D. E., & Haseltine, W. A. (1981) *Proc. Natl. Acad. Sci. U.S.A. 78*, 3388–3392.

Liu, F.-T., & Yang, N. C. (1978) *Biochemistry 17*, 4865–4876.

Mitchell, D. L., & Clarkson, J. M. (1981) *Biochim. Biophys. Acta 655*, 54–60.

Mitchell, D. L., & Clarkson, J. M. (1984) *Photochem. Photobiol. 40*, 735–741.

Mitchell, D. L., & Rosenstein, B. S. (1987) *Photochem. Photobiol. 45*, 781–786.

Mitchell, D. L., Haipek, C. A., & Clarkson, J. M., (1985) *Mutat. Res. 143*, 109–112.

Nishio, T., Katoh, A., Omote, Y., & Kashima, C. (1978) *Tetrahedron Letts. 18*, 1543–1544.

Nishio, T., Kato, A., Kashima, C., & Omote, Y. (1980) *J. Chem. Soc., Perkin Trans. 1*, 607–610.

Nishio, T., Katahira, K., & Omote, Y. (1981) *J. Chem. Soc. Perkin Trans. 1*, 943–946.

Noggle, J. H., & Schirmer, R. E. (1971) *The Nuclear Overhauser Effect: Chemical Applications*, Academic, New York.

Patrick, M. H. (1970) *Photochem. Photobiol. 11*, 477–485.

Rosenstein, B. S., & Mitchell, D. L. (1987) *Photochem. Photobiol. 45*, 775–780.

Rycyna, R. E., & Alderfer, J. L. (1985) *Nucleic Acids Res. 13*, 5949–5963.

Saenger, W. (1984) *Principles of Nucleic Acid Structure*, Springer-Verlag, New York.

Shoolery, J. N. (1959) *J. Chem. Phys. 31*, 1427–1428.

Taylor, J.-S., & Cohrs, M. P. (1987) *J. Am. Chem. Soc. 109*, 2834–2835.

Taylor, J.-S., Garrett, D. S., & Wang, M. J. (1988) *Biopolymers* (in press).

Ulmas, M. E., Franklin, W. A., Chan, G. L., & Haseltine, W. A. (1985) *Photochem. Photobiol. 42*, 265–273.

Varian XL-300 Series NMR Spectrometer System Advanced Operation Manual (1984) Varian Associates, Palo Alto, CA.

Vinter, J. G., Davis, A., & Saunders, M. R. (1987) *J. Comput.-Aided Mol. Des. 1*, 31–51.

Wang, S. Y., Ed. (1976) *Photochemistry and Photobiology of Nucleic Acids*, Vols. 1 and 2, Academic, New York.

Weinges, K., Kasel, W., Huber-Patz, H., Rodewald, H., & Irngartinger, H. (1984) *Chem. Ber. 117*, 1871–1876.

Weinges, K, Klein, J., Sipos, W., Gunther, P., Huber-Patz, U., & Rodewald, H. (1986) *Chem. Ber. 119*, 1540–1545.